2020 59th IEEE Conference on Decision and Control (CDC)
Jeju Island, Republic of Korea, December 14-18, 2020

Limit Cycle Oscillation Suppression Using a Closed-loop Nonlinear Active Flow Control Technique

Krishna Bhavithavya Kidambi[1], William MacKunis[2], and Anu Kossery Jayaprakash[2]

Abstract— **This paper presents a nonlinear control method, which achieves simultaneous fluid flow velocity control and limit cycle oscillation (LCO) suppression in a flexible airfoil. The proposed control design is based on a dynamic model that incorporates the fluid structure interactions (FSI) in the airfoil. The FSI describe how the flow field velocity at the surface of a flexible structure gives rise to fluid forces acting on the structure. In the proposed control method, the LCO are controlled via control of the flow field velocity near the surface of the airfoil using surface-embedded synthetic jet actuators. Specifically, the flow field velocity profile is driven to a desired time-varying profile, which results in a LCO-stabilizing fluid forcing function acting on the airfoil. A Lyapunov-based stability analysis is used to prove that the active flow control system asymptotically converges to the LCO-stabilizing forcing function that suppresses the LCO. Numerical simulation results are provided to demonstrate the performance of the proposed active flow-and-LCO suppression method.**

I. Introduction

The interaction between a flexible structure and the fluid surrounding it is referred to as fluid structure interactions (FSI). A detailed understanding of FSI is of critical importance in numerous applications in aeronautical and aerospace systems, petroleum and chemical industries, renewable energy systems, and others [1], [2], [3], [4]. A particularly important application of FSI is in the development of limit cycle oscillation (LCO) suppression control systems for aircraft. Indeed, a thorough understanding of the FSI and LCO can lead to significant improvements in the aerodynamic characteristics of aircraft, such as drag reduction and lift enhancement. While standard LCO suppression control in aircraft wings is achieved using deflection surfaces (e.g., ailerons, rudders), the contribution of this paper is the analysis of a control system that achieves LCO suppression via control of the wing boundary-layer flow field.

LCO (or flutter) are self-excited aeroelastic instabilities that can have a detrimental effect on aircraft flight performance and can even lead to catastrophic failures [5], [6], [7]. A thorough review of research and development in LCO suppression technology over 50 years is presented in [5]. Aerodynamic performance characteristics such as increased lift and delayed stall can be improved through control of the flow over the wing by considering the FSI. To implement flow control in an LCO suppression application, surface-embedded flow actuators can be employed to influence the flow dynamics near the wing boundary-layer.

Synthetic jet actuators (SJA) have been widely used in recent flow control and LCO suppression research. In [7], a SJA-based output feedback control method is presented that proves asymptotic regulation of LCO in small unmanned aerial vehicles UAVs. In [8], a numerical investigation of active flow control using SJAs is presented. A primary challenge in SJA-based control design is that the input-output characteristic of the SJA is nonlinear and contain parametric uncertainty. Additional challenges arise in designing flow control systems based on reduced-order mathematical models of the flow dynamics.

Active flow control techniques have been presented in numerous recent research results [9], [10], [11], [12]. A key challenge in designing control laws for fluid flow is that the governing dynamic equations are partial differential equations (PDEs) (e.g., Navier-Stokes equations), which are not amenable to control design. Proper orthogonal decomposition (POD)-based model order reduction is a popular technique, which can be used to express the Navier-Stokes PDEs as a finite set of ordinary differential equations (ODEs) [13], [14]. In the POD-based method, the nonlinear Navier-Stokes equations are projected onto a finite-dimensional subspace using Galerkin technique so that the projection error is minimized. The resulting reduced-order model is expressed as a set of nonlinear ordinary differential equations (ODEs), which are amenable to control design.

The contribution of this paper is the development of a nonlinear control method, which is rigorously proven to simultaneously control the boundary-layer flow dynamics and suppress the LCO in an aircraft wing section. To achieve the result, an LCO dynamic model is utilized, which incorporates FSI through a fluid forcing function. The fluid forcing function is in turn a function of the fluid flow velocity, which is controlled using surface-embedded SJAs. A POD-based reduced-order model for the actuated flow dynamics is used to develop a detailed tracking error system, and a rigorous Lyapunov-based stability analysis is utilized to prove that the flow control law drives the fluid forcing function to an offline-designed (desired) LCO-stabilizing fluid forcing function. Numerical simulation results are also provided, which incorporate detailed models of the LCO and reduced-order flow dynamics.

II. Mathematical Model

In this section, the mathematical model for the LCO dynamics and flow field dynamics are presented. Section II-A describes the LCO dynamics of a foil in the presence of

[1]Krishna Bhavithavya Kidambi is with Institute for Systems Research, University of Maryland, College Park, MD 20742. kidambi@umd.edu
[2]William MacKunis, Anu Kossery Jayaprakash are with Physical Sciences Department, Embry Riddle Aeronautical University, Daytona Beach, FL 32114. mackuniw@erau.edu, kosserya@my.erau.edu

978-1-7281-7447-1/20/$31.00 ©2020 IEEE

fluid forces. Next, a POD-based model reduction technique is utilized to recast the incompressible Navier-Stokes equations as finite set of nonlinear ODEs. The reduced-order model for the actuated flow dynamics will be utilized to develop the proposed closed-loop control system.

A. LCO Dynamic Model

The equation of motion describing the LCO dynamics, in the presence of a fluid forcing function are expressed as [15]

$$M(s)\ddot{q}(s,t) + C(\dot{q}(s,t)) + K(q(s,t)) = BF_{fluid}(s,t) \quad (1)$$

where $q(t) \triangleq \begin{bmatrix} h(t) & \eta(t) \end{bmatrix}^T \in \mathbb{R}^2$ denotes the LCO displacement vector containing plunging ($h(t)$) and pitching ($\eta(t)$) displacements, $s \in \mathbb{R}$ is the linear position along the structure (i.e., wing), $M(s) \in \mathbb{R}^{2\times 2}$ is the inertia matrix of the wing, and $C(*) \in \mathbb{R}^2$ and $K(*) \in \mathbb{R}^2$ denote viscous damping and stiffness functions, respectively. In (1), $F_{fluid}(s,t) \in \mathbb{R}$ denotes the fluid forces acting on the wing (i.e., a "virtual" control input), and $B \in \mathbb{R}^2$ is a constant input gain vector.

In the LCO dynamic model given by (1), the fluid forcing function $F_{fluid}(s,t)$ can be mathematically expressed as the product of the boundary-layer turbulence velocity $\upsilon(s,t)$ and a position-dependent function $b(s)$ as [15]

$$F_{fluid}(s,t) = b(s)\upsilon(s,t). \quad (2)$$

In (2) the fluid forcing function is directly dependent on the flow turbulence $\upsilon(s,t)$ near the surface of the wing. The variable s used in (2) is the linear position introduced in (1), and the function $b(s)$ in the fluid forcing function $F_{fluid}(s,t)$ can be expressed in terms of geometric and aerodynamic parameters as

$$b(s) = \rho d c_d U(s) \quad (3)$$

where ρ denotes the density of the air/fluid, d is the wing cross-sectional area, and c_d is the drag coefficient. In (3), $U(s)$ denotes the mean air flow velocity near the surface of the wing. The objective in this paper is to use wing surface-embedded SJAs to control the boundary layer flow perturbations $\upsilon(s,t)$ to track a desired time-varying profile that results in an LCO-suppressing fluid forcing function.

B. Flow Dynamics Reduced Order Model

In this section, a POD-based model reduction technique is utilized to recast the incompressible Navier-Stokes equations as a finite set of nonlinear ODEs. By expressing the Navier-Stokes PDEs as a set of ODEs, an approximate dynamic model for the flow dynamics will be obtained, which is more amenable to control design.

The incompressible Navier-Stokes equations are given as [16]

$$\nabla \cdot \upsilon = 0, \qquad \frac{\partial \upsilon}{\partial t} = -(\upsilon \cdot \nabla)\upsilon + \nu\nabla^2(\upsilon) - \nabla p, \quad (4)$$

where $\upsilon(s,t) : \Omega \times [0,\infty) \to \mathbb{R}$ denotes the velocity of the flow field over a spatial domain $s \in \Omega$; $p(s,t) \in \mathbb{R}$ is the space- and time-dependent pressure of the flow field over Ω; ∇ denotes the spatial gradient; and $\nu \triangleq \frac{1}{Re}$ is the kinematic viscosity, where Re denotes the Reynolds number.

In the POD-based model order reduction method, the flow field velocity $\upsilon(s,t)$ is expanded as a weighted sum of actuated and unactuated POD modes defined in the spatial domain Ω. The actuation effects are embedded in the coefficients of the Galerkin system. Specifically, the actuation effects can be included in the reduced-order model by defining the modal decomposition as [17], [18]

$$\upsilon(s,t) = \upsilon_0(s,t) + \sum_{i=1}^{n} x_i(t)\phi_i(s) + \sum_{i=1}^{m} \gamma_i(t)\psi_i(s) \quad (5)$$

In (5), $\phi_i(s) \in \mathbb{R}$ denote the POD modes; $x_i(t)$, $i = 1, ..., n$, are time-varying coefficients resulting from the modal decomposition; and $\upsilon_0(s,t) \in \mathbb{R}$ denotes the mean flow velocity over Ω, where $\psi_i(s) \in \mathbb{R}$ denote the actuation modes, and $\gamma_i(t) \in \mathbb{R}$ denote actuation values (i.e., control inputs). Physically, the actuation values could represent the controllable flow perturbations due to synthetic jet actuators, for example [19].

C. Reduced-order Model for the Actuated Flow

For the control design presented here, it will be assumed that an input separation method [18] is utilized to expand the flow field in terms of baseline (unactuated) POD modes and actuation modes. The following two subsections provide details on the reduced-order model for actuated flow that is being considered in this paper.

1) Actuated Dynamic Model: By substituting the actuated modal decomposition in (5) into (4), the actuated reduced-order flow dynamics can be expressed in terms of an auxiliary ("virtual") control input $u(t)$ as

$$\dot{x} = f(x) + g(x)u, \qquad y = h(x) \quad (6)$$

where $x(t) \triangleq [x_1(t),\ x_2(t), ...,\ x_n(t)]^T \in \mathbb{R}^n$ contains the unmeasurable coefficients resulting from POD-based model order reduction, $g(x) \in \mathbb{R}^{n\times m}$ ($m \geq n$) is an input gain matrix, $u(t) \triangleq [u_1(t), ..., u_m(t)]^T \in \mathbb{R}^m$ denotes a subsequently defined virtual control input (e.g., resulting from m arrays of synthetic jet actuators), and $y(t) \in \mathbb{R}^p$ is the measurable output (e.g., sensor measurements of flow field velocity or pressure). A detailed derivation of actuated reduced-order model in (6) can be found in [20], [18] and is omitted here for brevity.

In the subsequent flow control design and analysis, the controller development will be presented using a virtual control signal $u(t) \in \mathbb{R}^m$, which is defined via the parameterization

$$g(x)\,u = Q_{ain}(x,\gamma) + Q_{in}(\gamma,\gamma). \quad (7)$$

Remark 1: In (7), the terms $Q_{ain}(x,\gamma)$, $Q_{in}(\gamma,\gamma) \in \mathbb{R}^n$ are quadratic in their respective arguments. Since the $\gamma(t)$ dependence is quadratic in this case, the mapping between $\gamma(t)$ and $u(t)$ will not be unique in general; but the subsequent discussion is based on the assumption that the desired, commanded control input can be delivered by the virtual control signal.

Property 1: If $x(t) \in \mathcal{L}_\infty$, then the first and second partial derivatives of $f(x)$, $g(x)$, and $h(x)$ with respect to $x(t)$ exist and are bounded. Based on the flow measurement equation and the actuated flow dynamics in (6), $f(x)$ and $h(x)$ can be expressed as $f(x) \triangleq (L + \sum_{i=1}^{n} x_i Q_i)x$ and $h(x) \triangleq Cx$, where $L, Q_i \in \mathbb{R}^{n\times n}$ contain constant parameters resulting from POD; and the product $x_i Q_i$ is calculated element-wise.

The subsequently defined simulation model in Equation (41) provides a specific example of a POD-based flow dynamic model in this form. Detailed derivations of $f(x)$ and $h(x)$ in (6) can be found in [21].

III. SJA-based Control Model Derivation

In this section, the POD-based reduced-order model for the actuated flow dynamics will be augmented to include the effects of SJA actuation. To this end, a well-accepted, empirical model for the virtual surface deflection generated by SJA actuators [22] will be utilized to express the SJA-actuated flow dynamics in a control-oriented form, which explicitly includes the parametric uncertainty inherent in the SJA actuator model.

Remark 2: **(SJA in Flow Control)** The actuation term $u(t)$ in the flow dynamics in (6) is assumed to be generated by means of the virtual deflection angle resulting from an array of SJAs. For further details on the use of SJA in flow control applications, the reader is referred to [22].

A. SJA Actuator Model

The virtual deflection angle generated by an array of m SJAs (i.e., $u(t)$ in (6)) can be expressed as [22]

$$u_i(t) = \theta_{2i}^{\star} - \frac{\theta_{1i}^{\star}}{v_i(t)}, \qquad i = 1, 2, ..., m. \tag{8}$$

In (8), $v_i(t) \triangleq A_{ppi}^2(t) \in \mathbb{R}^+$ denotes a measurable input signal, where A_{ppi} represents the peak-to-peak voltage magnitude applied to the i^{th} SJA array; and $\theta_{1i}^{\star}$, $\theta_{2i}^{\star} \in \mathbb{R}$ are uncertain positive parameters. The SJA actuator model given in (8) illustrates one of the main challenges in SJA-based estimator and control design: the virtual surface deflection control input $u_i(t)$ depends nonlinearly on the SJA voltage input signal $v_i(t)$ and contains parametric uncertainty due to $\theta_{1i}^{\star}$ and $\theta_{2i}^{\star}$. To address these challenges, the voltage input signal $v_i(t)$ can be designed using the robust-inverse control structure [19]

$$v_i(t) = \frac{\hat{\theta}_{1i}}{\hat{\theta}_{2i} - u_{di}(t)} \tag{9}$$

where, $\hat{\theta}_{1i}$, $\hat{\theta}_{2i} \in \mathbb{R}^+$ are constant, *best-guess* feedforward estimates of the uncertain parameters $\theta_{1i}^{\star}$ and $\theta_{2i}^{\star}$. In (9), $u_{di}(t) \in \mathbb{R}$, for $i = 1, ..., m$, are subsequently defined auxiliary control signals. Note that (9) can be implemented using a singularity avoidance algorithm [23].

After substituting (8) and (9) into (6), the SJA-based control model can be expressed as

$$\dot{x} = f(x) + \Xi_B + \Omega u_d(t) \tag{10}$$

where $u_d(t) \triangleq [u_{d1}(t), ..., u_{dm}(t)]^T \in \mathbb{R}^m$, and expressions for the uncertain constant auxiliary terms $\Xi_B \in \mathbb{R}^m$ and $\Omega \in \mathbb{R}^{n\times m}$ can be readily obtained. To handle the uncertainty in the input-multiplicative matrix Ω in (10), the auxiliary control signal $u_d(t)$ is designed as

$$u_d(t) = \hat{\Omega}^{\#}\mu(t) \tag{11}$$

where $\hat{\Omega} \in \mathbb{R}^{n\times m}$ denotes a feedforward estimate of Ω, and $[\cdot]^{\#}$ denotes the pseudoinverse of a (nonsquare) matrix. Note that the standard matrix inverse operation could be used in place of the pseudoinverse for the case where $n = m$. In (11), $\mu(t) \in \mathbb{R}^n$ denotes a known, nominal, measurable control input signal. After substituting (11) into (10), the open loop SJA-based system can be expressed as

$$\dot{x} = f(x) + \Xi_B + \tilde{\Omega}\mu(t) \tag{12}$$

where $\tilde{\Omega} \triangleq \Omega\hat{\Omega}^{\#} \in \mathbb{R}^{n\times n}$. Heuristically, the uncertain matrix $\tilde{\Omega}$ represents the deviation between the actual SJA parameters $\theta_{1i}^{\star}$ and their constant estimates $\hat{\theta}_{1i}$, for $i = 1, ..., m$.

Property 2: The uncertain matrix $\tilde{\Omega}$ can be decomposed as

$$\tilde{\Omega} = I_n + \Delta(t) \tag{13}$$

where $I_n \in \mathbb{R}^{n\times n}$ denotes the identity matrix, and $\Delta(t) \in \mathbb{R}^{n\times n}$ denotes uncertain "mismatch" matrix.

Assumption 1: Approximate model knowledge is available such that the mismatch matrix Δ satisfies

$$\|\Delta(t)\|_{i\infty} < \varepsilon \tag{14}$$

where $\varepsilon \in \mathbb{R}^+$ is a known bounding constant, and $\|\cdot\|_{i\infty}$ denotes the induced infinity norm of a matrix. Heuristically, Inequality (14) can be interpreted as the assumption of approximate SJA model knowledge.

Preliminary results show that Assumption 1 is mild in the sense that the proposed control method performs well over a wide range of SJA parametric uncertainty.

By substituting (13) into (12), the SJA-based flow dynamic model can be expressed as

$$\dot{x} = f(x) + \Xi_B + \mu(t) + \Delta(t)\mu(t), \qquad y = Cx, \tag{15}$$

where the output matrix $C \in \mathbb{R}^{1\times n}$ for the single output case.

Remark 3: The control objective in this paper is based on driving the fluid forcing function to a desired fluid forcing function, which is designed in a separate step based on the objective of regulating LCO. The fluid forcing function in (2) can be approximated using POD as

$$F_{fluid} = b(s)v(s,t) \simeq b(s)y(t) = b(s)Cx(t), \tag{16}$$

where $y(t)$ is the output of the flow dynamic model described in (15). The approximation accuracy can be made arbitrarily accurate by adjusting the number of POD modes which are defined in (5).

IV. Control Development

The control objective is to design the control signal $\mu(t)$ to regulate the fluid forcing function F_{fluid} defined in (16) to a desired fluid forcing function $F_{fluid,des}$, which is defined as

$$F_{fluid,des} = b(s)y_d(t) \tag{17}$$

where $y_d(t)$ is the desired flow field velocity output that suppresses LCO. To quantify the control objective, a tracking error $e(t) \in \mathbb{R}$ and an auxiliary tracking error $r(t) \in \mathbb{R}$ are defined as

$$e(t) = F_{fluid} - F_{fluid,des}, \qquad r(t) = \dot{e} + \alpha e, \tag{18}$$

where $\alpha \in \mathbb{R}$ is a positive, constant control gain. Thus, the control objective can be stated mathematically as

$$e(t) \to 0. \tag{19}$$

A. Open Loop Error System

Taking the time derivative of $r(t)$ and using the definition of (18), the open loop error dynamics can be expressed as

$$\dot{r} = b(s)C\Big[\tfrac{\partial f(x)}{\partial x}\dot{x} + \tilde{\Omega}\dot{\mu}(t) + \dot{\Delta}(t)\mu(t)\Big] - \ddot{F}_{fluid,des} + \alpha(r - \alpha e), \tag{20}$$

where the constant uncertain matrix $\tilde{\Omega}$ is defined in (12). The error dynamics in (20) can be rewritten as

$$\dot{r} = \tilde{N}(t) + N_d(t) + \tilde{\Omega}_1\dot{\mu}(t) + b(s)C\dot{\Delta}(t)\mu(t) - e, \tag{21}$$

where $\tilde{\Omega}_1 \equiv b(s)C\tilde{\Omega}$ and the unknown, unmeasurable auxiliary functions, $\tilde{N}(t)$, $N_d(t) \in \mathbb{R}$ are defined as

$$\tilde{N} = b(s)C\tfrac{\partial f(x)}{\partial x}\dot{x} + \alpha(r - \alpha e) + e, \tag{22}$$

$$N_d = -\ddot{F}_{fluid,des} \tag{23}$$

Assumption 2: Approximate model knowledge is available such that the mismatch matrix $\dot{\Delta}(t)$ satisfies

$$b(s)C\left\|\dot{\Delta}(t)\right\|_{i\infty} < \varepsilon_1 < 1 \tag{24}$$

where $\varepsilon_1 \in \mathbb{R}^+$ is a known bounding constant, and $\|\cdot\|_{i\infty}$ denotes the induced infinity norm of a matrix.

The motivation for the separation of terms in (21), (22) and (23) is based on the fact that the following inequalities can be developed

$$|\tilde{N}| \le \rho(\|z\|)\|z\|, \qquad |N_d| \le \zeta_{N_d}, \qquad |\dot{N}_d| \le \zeta_{\dot{N}_d}, \tag{25}$$

where $\zeta_{N_d}, \zeta_{\dot{N}_d} \in \mathbb{R}^+$ are known bounding constants; $\rho(\cdot)$ is a positive, globally invertible, non-decreasing function; and $z(t) \in \mathbb{R}^2$ is defined as

$$z(t) \triangleq \begin{bmatrix} e(t) & r(t) \end{bmatrix}^T. \tag{26}$$

Note that the upper bound on $|\tilde{N}(t)|$ in (25) can be derived from (22) by using Property 1 along with the definitions in (16), (17), and (18).

B. Closed-Loop Error System

Based on the open-loop error system dynamics in (20), the control $\mu(t)$ is defined via

$$\dot{\mu}(t) = -k_u\|\mu(t)\|sgn(r) - (k_s + 1)r - \beta sgn(r) \tag{27}$$

where $k_u, k_s, \beta \in \mathbb{R}$ are positive, constant control gains.

Remark 4: The control design in (27) includes measurements of the tracking error derivative (i.e., $\dot{e}(t)$). This deficit can be remedied through the use of an observer; however, the observer design and analysis are omitted here to avoid distraction from the focus of the current result.

After substituting (27) into (20), the closed-loop error dynamics is rewritten as

$$\dot{r} = \tilde{N} + N_d - \tilde{\Omega}_1 k_u\|\mu(t)\|sgn(r) - \tilde{\Omega}_1(k_s + 1)r - \tilde{\Omega}_1\beta sgn(r) + b(s)C\dot{\Delta}(t)\mu(t) - e. \tag{28}$$

V. Stability Analysis

Theorem 1: The robust nonlinear control law given in (9), (11), and (27) ensures that all system signals remain bounded throughout closed-loop operation, and that the fluid forcing function tracking error is asymptotically regulated in the sense that

$$\|e(t)\| \to 0 \qquad \text{as} \qquad t \to \infty, \tag{29}$$

provided the control gain k_u, k_s and β introduced in (27) are selected according to the conditions

$$k_s > \frac{\rho^2(\|z\|)}{4(1-\varepsilon)min(\alpha, 1-\varepsilon)}, \; k_u \geqslant \frac{\varepsilon_1}{1-\varepsilon}, \; \beta \geqslant \frac{\zeta_{N_d}}{1-\varepsilon}. \tag{30}$$

Proof: Let $V(z,t) : \mathbb{R}^2 \to \mathbb{R}$ be a positive-definite function defined as

$$V = \frac{1}{2}e^2 + \frac{1}{2}r^2 \tag{31}$$

After taking the time derivative of (31) and using (13), (18) and (28), $\dot{V}(z,t)$ can be expressed as

$$\dot{V}(z,t) = -\alpha e^2 + r\tilde{N} + rN_d - r\tilde{\Omega}_1 k_u\|\mu(t)\|sgn(r) - r\tilde{\Omega}_1(k_s + 1)r - r\tilde{\Omega}_1\beta sgn(r) + b(s)rC\dot{\Delta}(t)\mu(t). \tag{32}$$

By using Assumptions 1 and 2, Property 2, the bounding inequalities in (22) and (23), and the gain conditions in (30), the expression in (32) can be upper bounded as

$$\dot{V}(z,t) \le -\left[min(\alpha, 1-\varepsilon) - \frac{\rho^2(\|z\|)}{4(1-\varepsilon)k_s}\right]\|z\|^2. \tag{33}$$

Provided the gain conditions in (30) is satisfied, (31) and (33) can be used to show that $V(t) \in \mathcal{L}_\infty$; hence, $e(t)$, $r(t) \in \mathcal{L}_\infty$. Given that $e(t)$, $r(t) \in \mathcal{L}_\infty$, a standard linear analysis technique can be used along with (18) to show that $\dot{e}(t) \in \mathcal{L}_\infty$. Since $e(t)$, $\dot{e}(t) \in \mathcal{L}_\infty$, (18) can be used along with the assumption that $y_d(t)$, $\dot{y}_d(t) \in \mathcal{L}_\infty$ to prove that $x(t)$, $\dot{x}(t) \in \mathcal{L}_\infty$. Given that $x(t)$, $\dot{x}(t) \in \mathcal{L}_\infty$, (6) can be used along with the Assumption 1 to prove that the control input $\mu(t) \in \mathcal{L}_\infty$. Since $r(t) \in \mathcal{L}_\infty$, Assumption 1 can be

used along with (27) to prove that $\dot{\mu}(t) \in \mathcal{L}_\infty$.

The definition of $V(z,t)$ in (31) can be used along with the inequality (33) to show that $V(z,t)$ can be upper-bounded as

$$\dot{V}(z,t) \leq -cV(z,t) \tag{34}$$

provided the sufficient condition in (30) is satisfied. The differential inequality in (34) can be expressed as

$$V(z,t) \leq V(z(0))e^{-ct}. \tag{35}$$

Hence, (26), (31) and (35) can be used to conclude that

$$\|e(t)\| \leq \|z(0)\|e^{-\frac{c}{2}t} \qquad \forall \ \ t \in [0,\infty). \tag{36}$$

■

VI. Simulation Results

A numerical simulation was performed to demonstrate the performance of the proposed control law. The simulation tests the capability of the proposed controller design in (27) to regulate the fluid forcing function in (2) to a desired fluid forcing function that suppresses the pitching and plunging LCO. Although the control design methodology in this paper is applicable to general systems with p sensor measurements and m control inputs, the simulation results address the specific case where $p = m = 1$ as a proof of concept.

A. LCO Dynamic Model

The LCO dynamic equation (cf. Equation (1)) used in the simulation can be expressed as

$$M_s\ddot{q} + C_s\dot{q} + K(q(t))\,q = BF_{fluid} \tag{37}$$

where $q(t) \triangleq \left[\begin{array}{cc} h(t) & \alpha(t) \end{array}\right]^T \in \mathbb{R}^2$ denotes the LCO displacement vector containing plunging ($h(t)$) and pitching ($\alpha(t)$) displacements, $F_{fluid}(t) \in \mathbb{R}$ is the fluid forcing function as defined in (2) and (3), and $B \in \mathbb{R}^2$ is a constant weighting matrix that depends on aerodynamic parameters. In (37), $M_s, C_s \in \mathbb{R}^{2\times 2}$ denote linear mass and damping matrices, respectively; and $K(q(t)) \in \mathbb{R}^{2\times 2}$ denotes a nonlinear stiffness matrix; all of which are explicitly defined as follows:

$$M_s = \left[\begin{array}{cc} m & mx_\alpha \\ mx_\alpha b & I_\alpha \end{array}\right], \qquad C_s = \left[\begin{array}{cc} C_h & 0 \\ 0 & C_\alpha \end{array}\right] \tag{38}$$

$$K(q(t)) = \left[\begin{array}{cc} K_h & 0 \\ 0 & K_\alpha(\alpha) \end{array}\right] \tag{39}$$

where the values of the aerodynamic and geometric parameters can be found in [7] and are omitted here for brevity. In (39), the nonlinear stiffness term $K_\alpha(\alpha)$ is explicitly defined as

$$K_\alpha = 2.82\left(1 - 22.1\alpha + 1315.5\alpha^2 - 8580\alpha^3 + 17290\alpha^4\right). \tag{40}$$

In (37), $F_{fluid}(t)$ is defined as in (2), where the values of the physical parameters can be found in [7]. The desired fluid forcing function $F_{fluid,des}(t)$ is generated via the control signal in a stable LCO model reference system.

B. Flow Dynamic Model

The reduced-order model for the flow dynamics in the simulation is in the form of (6). Specifically, the flow dynamic equations can be expressed as follows, where the POD parameters (see Property 1) can be found in [9]:

$$\begin{aligned}
\dot{x}_1 &= b_1 + L_{11}x_1 + Q_{141}x_1x_4 + Q_{111}x_1^2 + Q_{121}x_1x_2 \\
&\quad + Q_{131}x_1x_3 + u(t) \\
\dot{x}_2 &= b_2 + \left[L_{22} + t_2\left(x_2^2 + x_3^2\right)\right]x_2 + L_{23}x_3 + Q_{121}x_1x_2 \\
&\quad + u(t) \\
\dot{x}_3 &= b_3 + L_{32}x_2 + \left[L_{33} + t_3\left(x_2^2 + x_3^2\right)\right]x_3 + Q_{313}x_1x_3 \\
&\quad + Q_{314}x_1x_4 + u(t) \\
\dot{x}_4 &= b_4 + L_{41}x_1 + L_{44}x_4 + Q_{444}x_4^2 + Q_{414}x_1x_4 \\
&\quad + Q_{424}x_2x_4 + Q_{434}x_3x_4 + u(t) \\
y &= c_1x_1 + c_2x_2 + c_3x_3 + c_4x_4.
\end{aligned} \tag{41}$$

The measurement equation coefficients $c_1, ..., c_4$ were all selected as 1 without loss of generality. The control gain values were selected as $k_s = 10$, $k_u = 0.1$, $\alpha = 0.5$, and $\beta = 2.25$. The control input $u(t)$ in the simulation is generated using the SJA formulation in Equations (8) and (9), where the actual SJA parameters $\theta_1^\star$, $\theta_2^\star$ deviate from the best-guess estimates by approximately 6%.

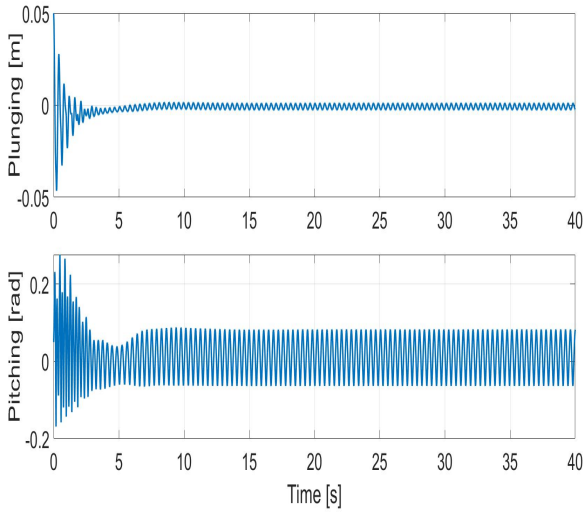

Fig. 1. Open-loop plunging and pitching response of the LCO system.

Fig. 1 shows the open-loop plunging and pitching responses of the LCO and Fig. 2 shows the closed-loop regulation of the LCO for six different initial conditions using the proposed control law. Fig. 3 shows the response of the actual and desired fluid forcing function during the closed-loop controller operation. The results clearly demonstrate the capability of the proposed control method to asymptotically regulate LCO via the control of the boundary-layer flow velocity.

VII. Conclusion

A nonlinear control method is developed, which is rigorously proven to asymptotically suppress LCO in a flexible

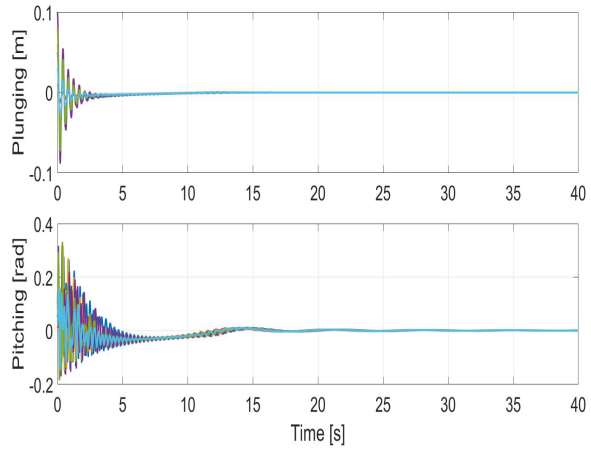

Fig. 2. Closed-loop response of the LCO plunging and pitching for six different initial conditions.

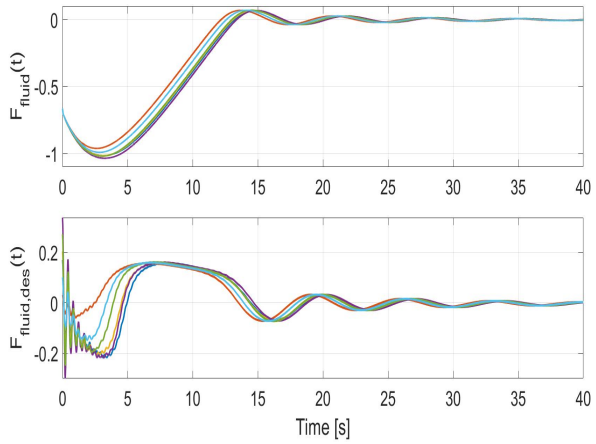

Fig. 3. Actual (top) and desired (bottom) fluid forcing functions during closed-loop controller operation for six different initial conditions.

wing section by using SJA to drive the wing boundary-layer flow velocity to a desired LCO-suppressing flow velocity profile. To achieve the result, a LCO dynamic model is utilized along with detailed mathematical models for the FSI, SJA, and the POD-based reduced-order flow dynamics. A Lyapunov-based stability analysis is utilized to prove asymptotic tracking of a desired LCO-suppressing fluid forcing function. Numerical simulation results are also provided, which demonstrate the capability of the proposed control method to achieve asymptotic regulation of LCO via boundary-layer flow control.

VIII. ACKNOWLEDGEMENT

This research is supported in part by NSF award number 1809790.

REFERENCES

[1] Z. A. Wei and Z. C. Zheng, "Fluid–structure interaction simulation on energy harvesting from vortical flows by a passive heaving foil," *Journal of Fluids Engineering*, vol. 140, no. 1, p. 011105, 2018.

[2] L. Ding, L. Zhang, C. Wu, X. Mao, and D. Jiang, "Flow induced motion and energy harvesting of bluff bodies with different cross sections," *Energy Conversion and Management*, vol. 91, pp. 416–426, 2015.

[3] Q. Xiao and Q. Zhu, "A review on flow energy harvesters based on flapping foils," *Journal of fluids and structures*, vol. 46, pp. 174–191, 2014.

[4] R. Parameshwaran, S. J. Dhulipalla, and D. R. Yendluri, "Fluid-structure interactions and flow induced vibrations: a review," *Procedia Engineering*, vol. 144, pp. 1286–1293, 2016.

[5] E. Livne, "Aircraft active flutter suppression: State of the art and technology maturation needs," *Journal of Aircraft*, vol. 55, no. 1, pp. 410–452, 2017.

[6] B. J. Bialy, I. Chakraborty, S. C. Cekic, and W. E. Dixon, "Adaptive boundary control of store induced oscillations in a flexible aircraft wing," *Automatica*, vol. 70, pp. 230–238, 2016.

[7] N. Ramos-Pedroza, W. MacKunis, and V. Golubev, "A robust nonlinear output feedback control method for limit cycle oscillation suppression using synthetic jet actuators," *Aerospace Science and Technology*, vol. 64, pp. 16–23, 2017.

[8] M. Kurowski, "Numerical simulation of a synthetic jet actuator for active flow control," in *Recent Progress in Flow Control for Practical Flows*, pp. 203–221, Springer, 2017.

[9] S. V. Gordeyev and F. O. Thomas, "A temporal proper decomposition (tpod) for closed-loop flow control," *Experiments in fluids*, vol. 54, no. 3, p. 1477, 2013.

[10] E. Caraballo, C. Kasnakoglu, A. Serrani, and M. Samimy, "Control input separation methods for reduced-order model-based feedback flow control," *AIAA journal*, vol. 46, no. 9, pp. 2306–2322, 2008.

[11] K. Taira, S. L. Brunton, S. T. Dawson, C. W. Rowley, T. Colonius, B. J. McKeon, O. T. Schmidt, S. Gordeyev, V. Theofilis, and L. S. Ukeiley, "Modal analysis of fluid flows: An overview," *Aiaa Journal*, pp. 4013–4041, 2017.

[12] R. Broglia, K.-S. Choi, P. Houston, L. Pasquale, and P. Zanchetta, "Output feedback control of flow separation over an aerofoil using plasma actuators," *International Journal of Numerical Analysis and Modeling*, 2018.

[13] M. Zhang and Z. C. Zheng, "Relations of pod modes and lyapunov exponents to the nonlinear dynamic states in flow over oscillating tandem cylinders," *Physics of Fluids*, vol. 30, no. 12, p. 123602, 2018.

[14] K. K. Nagarajan, S. Singha, L. Cordier, and C. Airiau, "Open-loop control of cavity noise using proper orthogonal decomposition reduced-order model," *Computers & Fluids*, vol. 160, pp. 1–13, 2018.

[15] A. Torrielli, F. Tubino, and G. Solari, "Effective wind actions on ideal and real structures," *Journal of Wind Engineering and Industrial Aerodynamics*, vol. 98, no. 8-9, pp. 417–428, 2010.

[16] G. Batchelor, *An introduction to fluid dynamics*. Cambridge university press, 2000.

[17] I. Akhtar, A. H. Nayfeh, and C. J. Ribbens, "On the stability and extension of reduced-order galerkin models in incompressible flows," *Theoretical and Computational Fluid Dynamics*, vol. 23, no. 3, pp. 213–237, 2009.

[18] C. Kasnakoğlu, R. C. Camphouse, and A. Serrani, "Reduced-order model-based feedback control of flow over an obstacle using center manifold methods," *Journal of Dynamic Systems, Measurement, and Control*, vol. 131, no. 1, p. 011011, 2009.

[19] W. MacKunis, S. Subramanian, S. Mehta, C. Ton, J. W. Curtis, and M. Reyhanoglu, "Robust nonlinear aircraft tracking control using synthetic jet actuators," in *52nd IEEE conference on decision and control*, pp. 220–225, IEEE, 2013.

[20] G. Lewin and H. Haj-Hariri, "Reduced-order modeling of a heaving airfoil," *AIAA journal*, vol. 43, no. 2, pp. 270–283, 2005.

[21] K. B. Kidambi, N. Ramos-Pedroza, W. MacKunis, and S. V. Drakunov, "A closed-loop nonlinear control and sliding mode estimation strategy for fluid flow regulation," *International Journal of Robust and Nonlinear Control*, vol. 29, no. 3, pp. 779–792, 2019.

[22] D. Deb, G. Tao, J. O. Burkholder, and D. R. Smith, "Adaptive synthetic jet actuator compensation for a nonlinear aircraft model at low angles of attack," *IEEE Transactions on Control Systems Technology*, vol. 16, no. 5, pp. 983–995, 2008.

[23] S. T. Mondschein, G. Tao, and J. O. Burkholder, "Adaptive actuator nonlinearity compensation and disturbance rejection with an aircraft application," in *American Control Conference (ACC), 2011*, pp. 2951–2956, IEEE, 2011.